Spectral-hole burning and carrier thermalization in GaAs at room temperature

S. Hunsche, H. Heesel, A. Ewertz, and H. Kurz
Institut für Halbleitertechnik II, Rheinisch Westfälische Technische Hochschule Aachen, Sommerfeldstrasse 24, 52074 Aachen, Germany

J. H. Collet
Laboratoire de Physique des Solides, Institut National des Sciences Appliquees, Avenue de Rangueil, 31077 Toulouse, France
(Received 7 May 1993; revised manuscript received 4 August 1993)

We report on femtosecond time-resolved transmission and reflectivity measurements on bulk GaAs. Spectral-hole burning is observed, to our knowledge, for the first time in GaAs at room temperature. Carrier thermalization occurs within 200 fs and shows no significant dependence on excitation density or excess energy in the range from 2×10^{17} cm^{-3} to 2×10^{18} cm^{-3} and 35 meV to 90 meV, respectively. Calculations of the carrier dynamics are performed and include full dynamic screening of the carrier-carrier and the carrier LO-phonon interaction. The calculated thermalization times agree well with the experimental results. Negative transmission changes above the spectral hole are mainly caused by a complementary increase of reflectivity, but not by an increase of absorption.

I. INTRODUCTION

The absorption of a short laser pulse with a central frequency above the band gap in a semiconductor creates free electrons and holes with an initial energy distribution that is essentially determined by the laser spectrum. On a very short time scale, this nonthermal energy distribution is transformed by carrier-carrier scattering into a Fermi-Dirac distribution, i.e., a quasiequilibrium is established that can be characterized by carrier temperatures and chemical potentials for the various bands. The time needed for this internal thermalization is of fundamental physical interest because it is closely related to the strength of the carrier-carrier interaction and determines critically nonlinear optical properties. Therefore the development of ultrashort laser pulses[1] has triggered much effort to clarify the initial stages of carrier relaxation (for a historical review see Ref. 2) and to detect nonthermal carrier distributions and the subsequent transition into the thermal regime. The temporal evolution of carrier-induced optical nonlinearities has been intensively studied in GaAs, AlGaAs, InP, and quantum well structures mainly by pump-probe[3–8] and time-resolved photoluminescence measurements.[9–13] Carrier-carrier scattering in bulk GaAs and quantum wells has also been studied by four-wave-mixing measurements of interband polarization dephasing,[14–16] and polarization rotation spectroscopy.[17,18] However, experiments on GaAs with 2 eV excitation pulses—derived from the widely used Rhodamine dye lasers—are complicated by concurrent ultrafast intervalley scattering.[19,20] Photoluminescence experiments with time resolutions down to 100 fs (Refs. 9–12) failed to show nonthermal distributions, except in the case of extremely low excitation density.[13]

In time-resolved differential transmission experiments, where the presence of carriers is measured via the bleaching of optical transitions, spectral-hole burning in the vicinity of the excitation energy was clearly observed in bulk GaAs at low temperature[3,21] and in quantum wells,[4,5] when the pump energy was close above the band gap.

Concerning the theoretical description of a photoexcited semiconductor, the temporal evolution outlined above corresponds to several levels of possible simplifications. In the earliest stage, as long as scattering processes are negligible, an exact description of population- and polarization-related effects is required. This regime can, in principle, be described by a nonequilibrium Green's function theory[22–28] or a density-matrix formalism.[29–31] This treatment becomes extremely complex when dephasing effects, mainly due to carrier-carrier collisions, have to be included. A general description of the transient dephasing regime is therefore very difficult and, to our knowledge, has not been attempted yet. Recently, a Monte Carlo method which includes polarization effects has also been developed that allows a simulation of the coherent regime.[32] However, as real carrier-scattering processes have not been included, a comparison between experiment and theory is not yet possible.

After dephasing of the optically excited electron-hole pairs, the temporal evolution of the free carriers can be described by kinetic Boltzmann equations for the single-particle distribution functions. These can be numerically solved either directly[33–35] or by Monte Carlo methods.[36–38] For comparison with experimental data, an additional model of the carrier-induced changes of the optical properties is required. Changes of the absorption are influenced by band filling, band-gap renormalization, and changes of the Coulomb enhancement and may not be readily interpreted as a direct measure of the carrier distributions.[7]

In this work, we present time-resolved differential

transmission spectra, which unambiguously show nonthermal features such as spectral-hole burning in bulk GaAs at room temperature. We calculate the temporal evolution of the optically injected carriers by solving the Boltzmann equations and calculate the associated absorption changes. The transient regime of carrier thermalization is investigated and compared with theoretical spectra for different excitation densities and excess energies. The kinetic description of the single-particle functions predicts thermalization times in close agreement with experimental data. The observed thermalization times are below 200 fs and do not change significantly in the density regime from 2×10^{17} cm^{-3} to 2×10^{18} cm^{-3} and for excitation energies between 1.46 eV and 1.51 eV. This result is also predicted by the calculations. Finally, we investigate the influence of reflectivity changes on the differential transmission spectra and conclude that they must be accounted for in order to interpret small variations of the differential transmission.

The paper is organized as follows. In Sec. II we give the experimental details and in Sec. III we describe the model used to calculate the carrier-induced absorption changes. In Sec. IV, we present the experimental and theoretical results and discuss the absorption theory in the nonthermalized regime, in particular the Coulomb enhancement. The results are summarized in Sec. V.

II. EXPERIMENTAL SETUP

The measurements are performed in a standard pump-probe setup. Pulses of a colliding pulse mode-locked dye laser with a wavelength of 620 nm are amplified in a six-pass dye amplifier pumped by a 7 kHz copper-vapor laser and focused in an ethylene-glycol cell to generate a "white-light" continuum which covers the spectral vicinity of the GaAs band gap. A fraction of this continuum, ranging from 1.4 eV to 1.8 eV, is used as a broadband probe pulse. The other part is spectrally filtered to obtain near-infrared pump pulses that are further amplified in a second amplifier stage similar to Ref. 39. A slit in a four prism sequence allows tunability from 1.45 eV to 1.57 eV, as well as chirp compensation, yielding near-infrared (NIR) pump pulses with 70 fs duration and a bandwidth of 23 meV.

The sample is a thin film of intrinsic GaAs ($d = 223$ nm), grown by molecular beam epitaxy and mounted on a thick BK-7 glass substrate. The precise film thickness has been determined from the Fabry-Pérot oscillations that occur in the linear transmission and reflectivity of the sample. The density of optically excited carriers is estimated from the maximum pump fluence assuming homogeneous excitation. This procedure is justified since the probe focus is kept much smaller than the pump spot and the sample thickness is much less than one absorption length. Measurements were performed for different excitation densities ranging from 2×10^{17} cm^{-3} to 2×10^{18} cm^{-3} and for different pump-photon energies between 1.46 eV and 1.51 eV. Pump-induced transmission or reflectivity changes are measured as differential transmission or reflectivity spectra (DTS, DRS), varying the time delay between pump and probe. The spectra are recorded by a diode array detector and an optical multichannel (OMA) system. We measure the chirp of the probe continuum,[40] which causes a frequency-dependent time delay offset. Chirp corrected spectra for a given time delay are obtained by interpolation between spectra measured at different delays, taking into account this offset. This numerical chirp correction of the measured spectra is *essential* to achieve a time resolution of some tens of femtoseconds. The probe bandwidth that is necessary to cover the whole range of significant transmission changes is too large to be completely chirp corrected by pulse compression. Even very careful pulse compression of the probe continuum would impose a considerable nonlinear chirp that results in a strongly frequency-dependent time delay at the edges of the spectrum.[40,41] This would clearly lead to a systematic error concerning the measured carrier dynamics.

III. THEORETICAL MODEL

Typical free-carrier dephasing times of highly excited semiconductors ($\rho_{\mathrm{exc}} \approx 10^{17}$ cm^{-3} or more) at room temperature are on the order of 10 fs.[14,42] Therefore a description of the carrier dynamics on a time scale of a few hundred femtoseconds may be restricted to the semiclassical regime, excluding coherent effects. In this approach, the state of the excited material is expressed in terms of distribution functions for electrons, heavy holes, light holes, and occupations of optical and acoustical phonons. We calculate the temporal evolution of the photogenerated electron-hole plasma by solving the Boltzmann equations that describe the kinetics of these one-particle distribution functions. The equations are nonlinear, as the scattering rates, which couple the equations for each type of particle, depend on the carrier distributions and therefore are time dependent. We use dynamically screened interaction potentials within the plasmon pole approximation to calculate the scattering rates. Details of the calculations are given in Refs. 33, 34 and 7.

To compare the calculated carrier dynamics with our experimental data, a model of the carrier-induced changes of the sample transmission is required. In a first approach, we neglect the influence of multiple interferences and reflectivity changes when analyzing the transmission data. This approximation is discussed and justified below. The sample transmission then reads

$$I_T \propto e^{-\alpha d}, \tag{3.1}$$

with the absorption coefficient α and the sample thickness d. The differential transmission for small changes ($\Delta\alpha d \ll 1$) is given by

$$\mathrm{DTS} = \frac{I_T(\Delta t) - I_T(-\infty)}{I_T(-\infty)} \simeq -\Delta\alpha d, \tag{3.2}$$

so that the measured spectra can be directly related to a model of the absorption coefficient of the excited material. We note that using this approximation may result in a relative error in $\Delta\alpha$ of a few percent.[43]

It has been previously pointed out that the carrier-induced absorption changes cannot be interpreted in terms of band filling alone. Band-gap renormalization and screening of the exciton and of the Coulomb enhancement for interband transitions have to be taken into account. We use basically the semiempirical model for the absorption of the excited material developed in Ref. 7, where the absorption coefficient close to the band edge is expressed as the sum of an excitonic and an interband contribution:

$$\alpha(\hbar\omega) = \alpha_{\mathrm{ex}}(\hbar\omega) + \alpha_{\mathrm{ib}}(\hbar\omega). \tag{3.3}$$

Assuming parabolic bands and a single effective valence band, the interband absorption can be written as

$$\alpha_{\mathrm{ib}}(\hbar\omega,\rho) = \alpha_0 \times \mathrm{CEF}(\hbar\omega,\rho) \times \sqrt{\hbar\omega - E_g(\rho)} \times\{1 - f_e[\Delta E_e(\hbar\omega)] - f_h[\Delta E_h(\hbar\omega)]\}, \tag{3.4}$$

where $E_g(\rho)$ is the band gap in the presence of an electron-hole plasma of density ρ, $\mathrm{CEF}(\hbar\omega,\rho)$ is the Coulomb enhancement factor[44–46] for the transition energy $\hbar\omega$, and f_e and f_h are the electron and hole distribution functions at the respective excess energies $\Delta E_e(\hbar\omega)$ and $\Delta E_h(\hbar\omega)$. The proportionality constant α_0 is taken as 2.5×10^4, which gives a good agreement with the unperturbed absorption $\alpha(\hbar\omega, \rho = 0)$ just above the band edge. The band-gap reduction ΔE_g and the CEF of the excited material are calculated with the model of Banyai and Koch.[44] These two quantities depend on the Debye-Hückel wave vector q_D which is computed with the actual carrier distributions to allow for nonequilibrium effects. However, the calcuations of both the band-gap reduction and the CEF do *not explicitly* take into account the actual carrier distributions. We assume a rigid band shift and neglect the k dependence of the band-gap renormalization.[47]

To include the collision broadening of the interband transitions, the absorption coefficient is convoluted with the line-shape function

$$B = \left[\pi \times \Gamma(\rho) \times \cosh\left(\frac{\hbar\omega}{\Gamma(\rho)}\right)\right]^{-1}, \tag{3.5}$$

with a density-dependent broadening

$$\Gamma(\rho) = 1.4 \times R_H(0) + 2 \times 10^{-18}\ \mathrm{cm}^3 \times \rho \times R_H(0). \tag{3.6}$$

The excitonic absorption is represented as a series of discrete transitions:

$$\alpha_{\mathrm{ex}}(\hbar\omega) = 4\alpha_0 R_H^{3/2}(\rho) \times \sum_{n=1}^{\infty} \frac{1}{n^3} \frac{\Gamma(\rho)}{\left(\hbar\omega - E_g(\rho,T) - \frac{R_H(\rho)}{n^2}\right)^2 + \Gamma(\rho)^2}, \tag{3.7}$$

where $R_H(\rho)$ is the exciton Rydberg constant in the presence of the electron-hole plasma of density ρ. $R_H(0)$ is the exciton Rydberg constant of the unexcited material. It is known from experimental data in bulk material that the absolute position of the lowest exciton state does not shift with carrier density below the Mott transition.[26,48] Therefore we assume that the reduction of the exciton binding energy equals the band-gap reduction $\Delta E_g(\rho,\mathrm{T})$ and use

$$R_H(\rho) = \begin{cases} R_H(0) + \Delta E_g & \text{if } R_H(0) + \Delta E_g \geq 0 \\ 0 & \text{if } R_H(0) + \Delta E_g < 0. \end{cases} \tag{3.8}$$

Note that ΔE_g is negative and that no bound exciton states exist when $R_H = 0$.

This simple model for the absorption should be regarded as a provisory compromise. We use the Banyai-Koch model for calculation of the CEF and the band-gap renormalization since it gives a reasonable shape of the absorption changes and satisfactory agreement of the signal amplitude in the thermal regime,[49] which is typically reached within 200 fs in our experiments (see below). Possible modifications of the CEF due to nonthermal carrier distributions, which can be accounted for in more sophisticated CEF models, will be discussed in Sec. IV C.

Our model will only allow a semiquantitative comparison with the experimental spectra due to the limited accuracy of the spectral shape of the Coulomb enhancement and the band-gap reduction. Therefore, as a first step, we consider it sufficient to compare the calculated spectra directly with the experimental DTS, according to Eq. (3.2), without including the influence of reflectivity variations and thin-film Fabry-Pérot effects.

IV. RESULTS AND DISCUSSION

A. General temporal evolution

Figures 1 and 2 show the general temporal evolution of the DTS for excitation at 1.46 eV and a pump intensity of 9 μJ/cm^2, giving a density of 2×10^{17} photoexcited carriers per cm^3. The presence of pump-excited carriers at a given point in k space causes bleaching of the corresponding optical transition leading to a positive signal in these spectra. Experimental curves are presented in Fig. 1 at delay times between -225 fs and -100 fs in steps of 25 fs and in Fig. 2(a) at delay times between -50 fs and 200 fs in steps of 50 fs. For comparison, Fig. 2(b) shows theoretical spectra calculated with identical excitation parameters for the same time delays as in Fig. 2(a).

At very early negative times (Fig. 1) the experimental spectra show oscillating structures around the exciton at 1.42 eV. We also observe weaker oscillations at the pump energy which, to our knowledge, have not been observed before in bulk GaAs. These oscillations are caused by the interaction of the pump laser field with the polarization induced by the probe pulse in the sample which leads to perturbed free induction decay and by

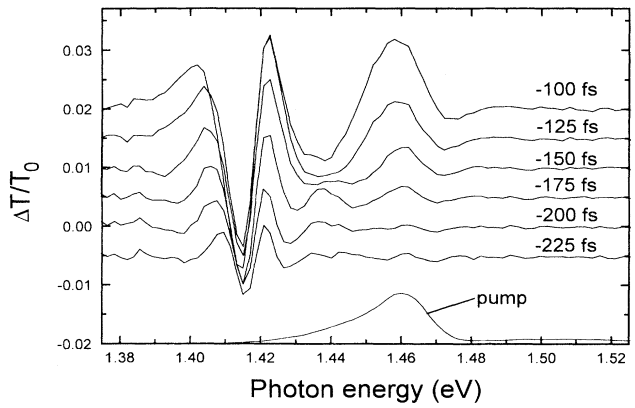

FIG. 1. Temporal evolution of differential transmission (DTS) for delay times from -225 fs to -75 fs in steps of 25 fs. The spectra are shifted for clarity. $\hbar\omega_{\text{pump}} = 1.46$ eV and $\rho_{\text{exc}} = 2 \times 10^{17}\text{cm}^{-3}$.

two-beam coupling between the pump and probe fields.[30] The main contribution to the observed oscillations will be due to the latter effect, as the free induction decay should become very weak for a slowly varying density of states. However, both effects lead to spectral oscillations with a period that is inversely proportional to the delay time and they can hardly be separated experimentally. We have not calculated the DTS for large negative delay times since these effects are not accounted for in our theory.

For excitation above the band edge, the occurrence of oscillations around the pump is determined by the ratio of the pulse duration and the intraband scattering rate Γ, which describes how fast the pump-excited carriers are scattered out of the optically coupled states.[50,51] If Γ is taken as the mean scattering rate for electrons and holes, respectively, Γ^{-1} is the optical dephasing time $T_2 = 2/(\Gamma_e + \Gamma_h)$.[35,52] Pulse durations shorter than Γ^{-1} are required to measure the oscillations around the pump energy.[50] Therefore we can estimate that the dephasing time for the transition at 1.46 eV is on the order of the pump-pulse width. While the oscillations around the pump are still weakly visible for excitation at 1.48 eV, we did not observe this effect when exciting at 1.51 eV. These results imply a strong energy dependence of the dephasing time in good agreement with the calculated *e-e*-scattering rates that are used in our plasma dynamics model. This is illustrated by Fig. 3, which shows the energy dependence of the theoretical *e-e*-scattering rates for different plasma densities. The calculations show a strong increase of the scattering rate with plasma density and excess energy up to 120 meV. An increase of the excess energy from 37 meV to 90 meV is associated by an increase of the scattering rates by roughly a factor 2, for all densities, which may explain the experimental findings.

Approaching time delay $\Delta t = 0$, the period of the oscillations around the pump and the exciton energy increases (Fig. 1) and during the pump-pulse duration a strong bleaching around the pump energy evolves, which is usually referred to as a "spectral hole." This indicates the buildup of a nonthermal carrier distribution around the excitation energy by absorption of pump photons. Light hole contributions to the spectral-hole burning (as reported in Ref. 53) cannot be observed for the experimental conditions of Fig. 1, as the valence band splitting is much smaller than the laser bandwidth. While there has been some evidence of an initial redshift of the spectral hole,[21] Fig. 1 unambiguously shows that in our experiment this signal is *initially peaked at the excitation energy*. However, within the pump-pulse duration the bleaching peak is drastically broadened on the

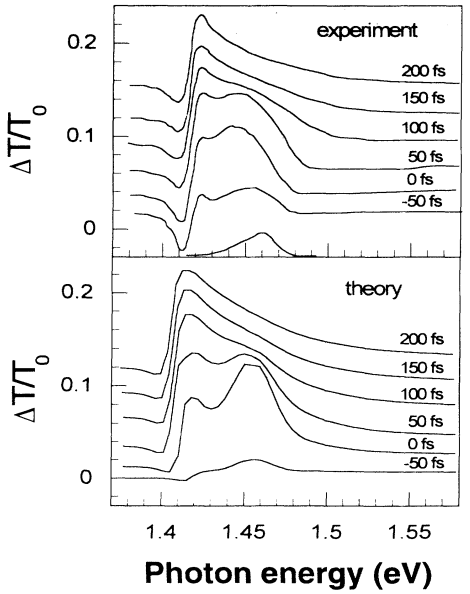

FIG. 2. (a) Experimental DTS between −50 fs and 200 fs in steps of 50 fs. Same excitation parameters as in Fig. 1(b) Theoretical spectra between −50 fs and 200 fs.

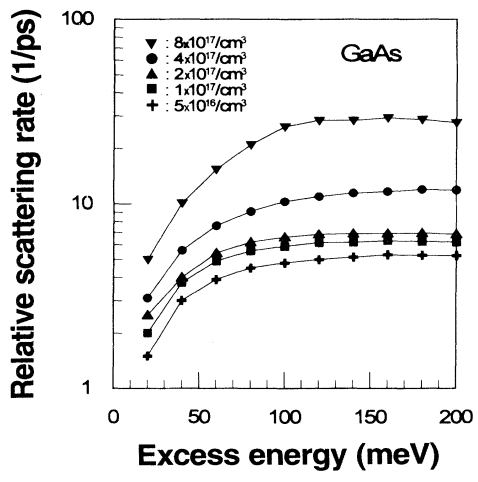

FIG. 3. Electron-electron scattering rate $R_{ee} = \frac{1}{f_e} \left.\frac{df}{dt}\right|_{ee}$ at the photogeneration energy versus excess energy at different plasma densities. The full width at half maximum of the carrier distribution is 20 meV.

low-energy side and extends to the band edge already at −50 fs, i.e., before the pump pulse maximum (Fig. 2). From −50 fs to +50 fs, the bleaching maximum shows a distinct shift of 20 meV towards the band edge. The spectra at this stage may be qualitatively described as a nonthermal bleaching peak on top of a broadband background, which cannot, on this time scale, be ascribed to a relaxed (i.e., thermalized) distribution of carriers. We stress that a direct interpretation of the DTS in terms of carrier distribution alone is not possible, because of the strong influence of changes of the CEF (Ref. 7) (see also end of Sec. IV C). In the interval from 1.4 to 1.43 eV, the calculated DTS result (Fig. 2) from a delicate balance between the induced absorption due to the gap shrinkage and the induced transmission due both to the exciton screening and to the reduction of the CEF. At delay time $\Delta t \leq 0$ fs, there is no significant contribution of the band filling in this spectral region. The theoretical results for the interval from 1.4 to 1.43 eV strongly depend on the CEF and band-gap model chosen. In the interval from 1.43 to 1.48 eV, the DTS are dominated by the band filling effect which is responsible for bleaching. We note that the calculated spectra reproduce well the occurrence and the broadening of the spectral hole, but underestimate the redshift of the peak position with increasing time delay. The observed shift on this time scale cannot be ascribed to a relaxation of carrier distributions. The possible influence of the CEF variations in the nonthermalized regime will be discussed in Sec. IV C.

After 100 fs the nonthermal signature decays and after 200 fs the spectra show a roughly exponential decrease of the differential transmission with increasing photon energy. The overall shape of the DTS does not change for longer delay times. This indicates that a thermal carrier distribution is established within 150–200 fs. The general temporal evolution of the DTS is very well described by the theoretical spectra shown in Fig. 2(b). However, it will be shown below that the DTS are primarily determined by the occupation of conduction band states, so that the DTS mainly give information on the electron dynamics. We conclude that our plasma dynamics model gives a correct description of the observed electron thermalization. It is important to add that, as in previous works,[7,54] the use of dynamically screened carrier interactions is essential for obtaining a realistic time evolution, because static screening underestimates the scattering rates and therefore predicts longer thermalization times.

In Fig. 4 the computed kinetics of the electron distribution function is displayed, according to the experimental conditions of Figs. 1 and 2. The photogeneration peak appears to be slightly shifted towards higher energies, because of the carrier-induced band-gap shrinkage, which corresponds to a shift of the energy axis in Fig. 4. The electron distribution resembles the pump spectrum at −50 fs, i.e., at the very beginning of the excitation pulse, but is already considerably broadened at 0 fs. The distribution is very close to a Maxwell-Boltzmann distribution at time delay 200 fs, with a thermal energy of $k_B T_e \simeq 30 - 35$ meV. The average energy per particle is therefore close to the initial photogeneration energy

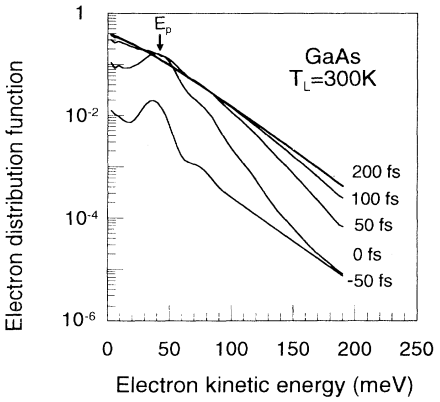

FIG. 4. Theoretical electron distribution functions calculated with the experimental parameters of Fig. 1.

$E_p = 40$ meV (with respect to the unrenormalized band gap). This is easily understood. First, there is no significant energy loss to the lattice within 200 fs, because E_p is only slightly larger than the threshold energy for LO-phonon emission, and the initial excess energy is rather close above the lattice temperature of 300 K. Second, the transfer of energy to the much cooler hole system via electron-hole scattering is not very efficient because of the large mass difference between electrons and holes. We conclude that the thermalization of the electron distribution is mainly due to electron-electron scattering, which is not accompanied by an energy loss of the electron system on this time scale.

The computed time evolution of the hole distribution function is displayed in Fig. 5. The widths of the initial photogeneration peak and the initial excess energy are much smaller than for electrons because of the smaller curvature of the hole band. Holes are generated with an average excess energy of 5 meV only. The calculations predict a strong absorption of LO phonons by the holes, giving rise to a second peak which is shifted by the energy $\hbar\omega_{\mathrm{LO}}$. This leads to an effective energy gain of the hole distribution already within the first 200 fs. Both peaks are strongly broadened during the excitation, but

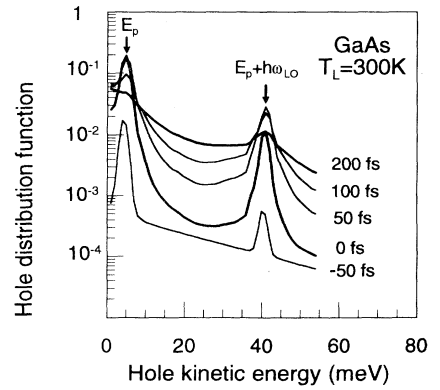

FIG. 5. Calculated hole distribution functions corresponding to Fig. 4.

the distribution is still nonthermal at time delay 200 fs. As the electrons do not lose energy on this time scale, it follows that the hole kinetics is mainly determined by LO-phonon absorption and hole-hole scattering. The calculations predict that thermalization of the hole distribution and of the whole electron-hole plasma occurs within several hundreds of femtoseconds, in accordance with Ref. 11. However, after some broadening of the initial hole distribution the occupation number f_h is much lower than the electron occupation f_e for total excess energies up to $\approx$100 meV. The DTS, which are proportional to (f_e+f_h), are therefore mainly determined by the electron distribution and do not provide a sensitive measure for the hole dynamics or the thermalization between electrons and holes.

B. Dependence on excitation parameters

In order to get a better understanding of the thermalization process, we performed a parametric study of the influence of excitation parameters. Both the excitation density and the excitation energy are varied. In Figs. 6–8, we compare the temporal evolution of experimental and theoretical DTS for pump energies of 1.46 eV, 1.48 eV, and 1.51 eV and various excitation densities between 2×10^{17} cm^{-3} and 2×10^{18} cm^{-3}. At 0 fs (Fig. 6), all experimental and calculated spectra clearly show a peak near the pump energy, indicating a nonthermal carrier distribution. As in Fig. 2, the amplitude of the calculated DTS agrees well with the experimental value, but the theory fails to reproduce the correct line shape and peak position. This discrepancy increases for higher excitation energies.

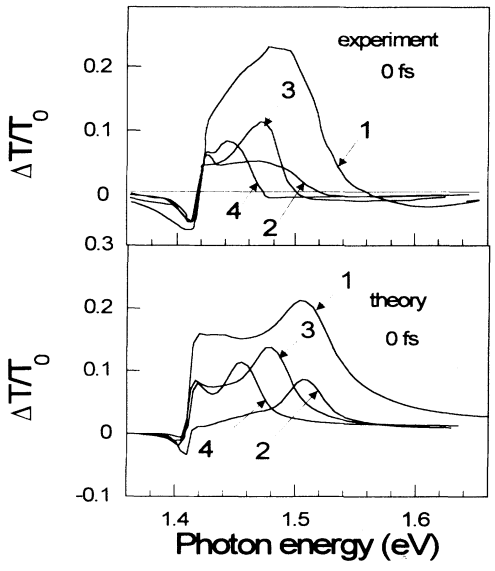

FIG. 6. Comparison of experimental and calculated DTS at delay time $\Delta t = 0$ fs for various excitation parameters. The spectra are labeled as 1: $\hbar\omega_{\rm pump} = 1.51$ eV, $\rho_{\rm exc} = 2 \times 10^{18}$ cm^{-3}; 2: $\hbar\omega_{\rm pump} = 1.51$ eV, $\rho_{\rm exc} = 3 \times 10^{17}$ cm^{-3}; 3: $\hbar\omega_{\rm pump} = 1.48$ eV, $\rho_{\rm exc} = 6 \times 10^{17}$ cm^{-3}; 4: $\hbar\omega_{\rm pump} = 1.46$ eV, $\rho_{\rm exc} = 2 \times 10^{17}$ cm^{-3}.

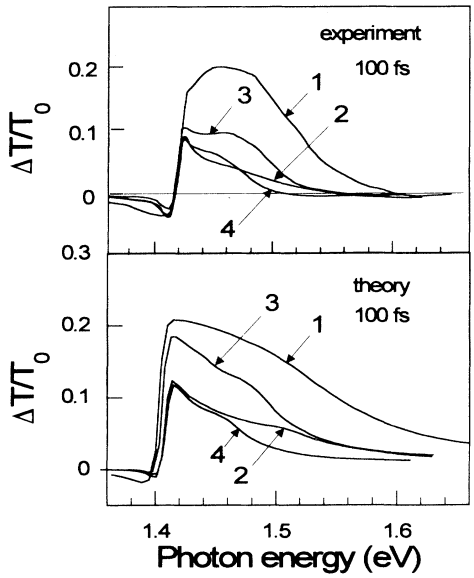

FIG. 7. Experimental and calculated DTS at delay time $\Delta t = 100$ fs. Excitation parameters and labeling of the spectra as in Fig. 6.

At 100 fs all spectra still exhibit a slight nonthermal feature (Fig. 7) that vanishes after 200 fs (Fig. 8). This applies to all excitation densities and pump energies we have studied. Spectra for similar densities become nearly identical after 200 fs, independent of the initial excess energy. This insensitivity of the thermalization times on excitation parameters is supported by the theoretical curves, which also show thermalization within 200 fs for all experimental conditions.

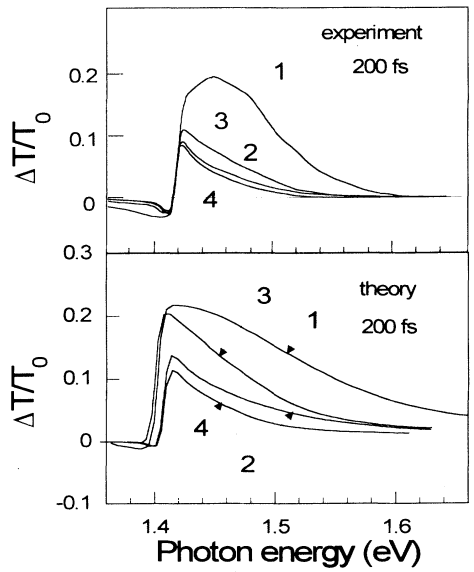

FIG. 8. Experimental and calculated DTS at delay time $\Delta t = 200$ fs. Excitation parameters and labeling of the spectra as in Fig. 6.

The observed independence of the thermalization time versus excess energy and carrier density can be explained by a subtle balance of scattering rate and energy distribution: An increase in excess energy means that carriers have to be distributed over a larger energy range during thermalization. Therefore a larger mean energy exchange per collision or a larger scattering rate at higher excess energies is required to explain a constant thermalization time. Indeed, in the energy range covered by our measurements, our calculations predict an increasing scattering rate with increasing energy (Fig. 3), thereby explaining the energy independence of the thermalization times.

We also observe that the thermalization time does not change with increasing carrier density. However, the total rate of carrier-carrier scattering (CCS) increases with increasing density. In principle, this would result in faster thermalization if the interaction strength remained unchanged. The insensitivity of the thermalization time with respect to the excitation density indicates a reduction of CCS efficiency with increasing density, which compensates the increasing scattering rate. This can be explained by the screening of the Coulomb interaction and by the increasing degeneracy of the plasma, i.e., Pauli blocking of scattering final states, which leads to a decrease of the CCS rates.[55]

C. Simultaneous transmission and reflectivity measurements

In the experimental spectra shown so far we observe during the nonthermal regime a small negative transmission change above the spectral hole (see Figs. 6 and 7), similar to the data in Ref. 21. However, this negative transmission change in our spectra is always a small effect ($\Delta T/T_0 \leq 1\%$) that may not be readily interpreted as an induced absorption using Eq. (3.2). The transmission change measured in DTS is, in principle, not entirely determined by absorption changes but is influenced by reflectivity changes as well.[56,57] In order to clarify the origin of the negative transmission change observed in our spectra, we performed simultaneous DTS and DRS measurements for a quantitative determination of absorption changes.

As the sample thickness is on the order of the light wavelength, the transmission, the reflectivity, and their respective changes due to changes in n and κ are strongly influenced by interference effects. (Here, n is the index of refraction and κ the extinction coefficient of the sample.) This applies in particular to the reflectivity changes. In fact, the magnitude as well as the sign of the reflectivity changes are dependent on the exact wavelength and film thickness. Precise determination of refractive and absorptive changes requires a careful investigation of simultaneously measured DTS and DRS including the correction for multiple interferences.

For the analysis of our experimental data, we use the procedure described in Ref. 58. The transmission and reflectivity changes for given changes of n and κ are given by

$$\Delta T = \frac{\partial T}{\partial n}\Delta n + \frac{\partial T}{\partial \kappa}\Delta\kappa \tag{4.1a}$$

and

$$\Delta R = \frac{\partial R}{\partial n}\Delta n + \frac{\partial R}{\partial \kappa}\Delta\kappa \tag{4.1b}$$

that can be solved for Δn and $\Delta\kappa$. Starting with the complete formula for transmission and reflectivity of a thin film,[58] we calculate the partial derivatives of R and T with respect to n and κ. The numerical values of these derivatives are evaluated for the spectral range covered by the measurements. In this procedure, we use data sets $n(\omega)$ and $\kappa(\omega)$ that are derived by an interpolation between literature data[59] and give a consistent fit of the static transmission and reflectivity of our sample. Finally, Eqs. (4.1) are solved to obtain precise data on the induced absorption change $\Delta\alpha$.

Figure 9 shows the experimental spectra and the calculated negative changes in the optical density $-\Delta\alpha d$ for excitation at 1.51 eV, at a density of 3×10^{17} cm^{-3} at a time delay of 75 fs after excitation. The DTS still clearly shows a nonthermal feature and a slight negative transmission change above 1.57 eV. We find that the qualitative interpretation of the strong bleaching in terms of carrier distribution remains valid, justifying the direct comparison of measured DTS and calculated absorption changes in the previous sections of this paper. However, it is obvious that the negative transmission change around 1.6 eV is mainly due to an increased reflectivity in this range. We conclude that our measurements show *no induced absorption* due to the nonthermal carrier distribution as reported in Ref. 21. This result has been confirmed by measurements with a sample with different thickness. We stress that the spectral shape of the DRS depends very strongly on the film thickness for partially transparent films with thicknesses on the order of a few hundred nm. This cannot be avoided by using an antireflection coating, since this minimizes R as a function of the coating thickness for a certain wavelength only. In addition, this minimum generally does not correspond to

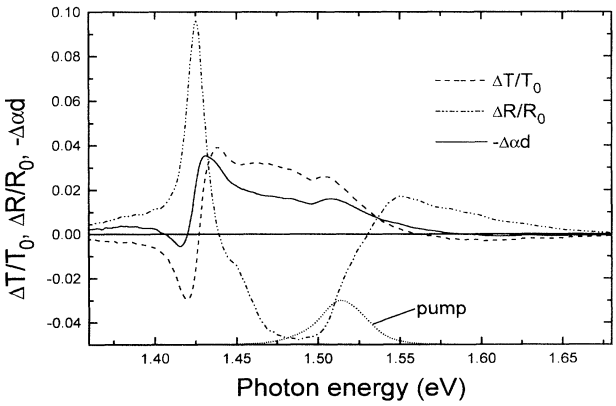

FIG. 9. Measured DTS and DRS for $\Delta t = 75$ fs, $\hbar\omega_{\text{pump}} = 1.51$ eV, $\rho_{\text{exc}} = 3\times10^{17}$ cm^{-3}, and negative absorption change $(-\Delta\alpha d)$, calculated from these measurements.

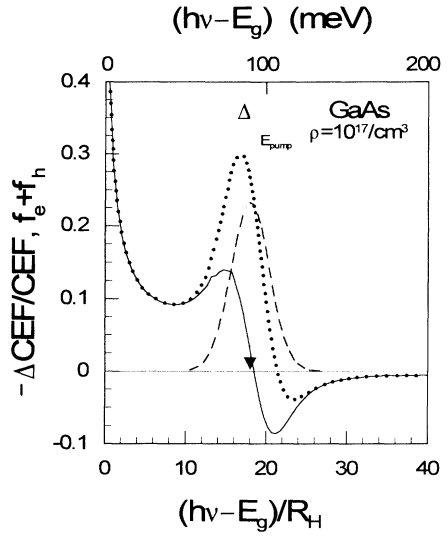

FIG. 10. Dotted line: Calculated normalized absorption change $(-\Delta\alpha/\alpha_0)$ according to Eq. (4.2) for Gaussian carrier distribution. Solid line: Contribution due to CEF change $-\Delta\mathrm{CEF}/\mathrm{CEF}(0)$. Dashed line: Occupation factor f_e+f_h.

zeros of the derivatives $\frac{\partial R}{\partial n}$ and $\frac{\partial R}{\partial \kappa}$ in Eq. (4.1b).

In order to study the possible influence of electron-hole correlations on the carrier-induced absorption changes, we performed CEF calculations that explicitly take into account the carrier distribution. From Eq. (3.4) it follows that for small variations the relative absorbance change can be expressed as

$$\frac{-\Delta\alpha}{\alpha(\rho=0)} \simeq \left(\frac{\Delta E_g(\rho)}{2\left[\hbar\omega - E_g(\rho)\right]} - \frac{\Delta\mathrm{CEF}(\hbar\omega,\rho)}{\mathrm{CEF}(\hbar\omega,0)} + \Delta f_e + \Delta f_h\right). \quad (4.2)$$

The CEF has been calculated in the framework of the factorization approximation,[60,61] using excitation parameters corresponding to the experimental situation of Fig. 9. In the thermalized regime, previous calculations showed a peak of the CEF around the Fermi energy for high plasma density.[46] In the nonthermalized regime, our calculations predict an oscillation of the CEF around the photogeneration energy, similar to the result of Ref. 26. A similar behavior has also been qualitatively predicted in Ref. 62, for an idealized physical situation. The occurrence of this effect depends critically on the density, which has to be high, and on the width of the electron distribution around the excitation energy, which has to be narrow. If the influence of the CCS is omitted during the pump pulse, the electron distribution reproduces the laser line shape, with a full width at half maximum (FWHM) of 25 meV. The curves shown in Fig. 10 are computed within this approximation. The solid line displays the quantity $-\Delta\mathrm{CEF}/\mathrm{CEF}$ at a density of 10^{17} cm^{-3}. The dashed line describes the energy dependence of the the corresponding occupation factor (f_e+f_h). The dotted curve shows the sum of these two contributions which is the dominant contribution to the absorbance change according to Eq. (4.2). The oscillatory behavior of the CEF around the photogeneration energy leads to a small redshift Δ of the bleaching maximum and a weak induced absorption, which is partially compensated by the bleaching due to the occupation factor. The calculation predicts an induced absorption of 4% at 120 meV excess energy, $\simeq$13% of the magnitude of the bleaching maximum. For our sample, this would correspond to a negative transmission change of approximately 1%.

In reality, CCS cannot be neglected, as it leads to a substantial broadening of the pump-excited carrier distribution even before the pump pulse maximum (see Fig. 4). This leads to a reduction of the CEF oscillation and to a much broader bleaching contribution to the DTS. We conclude that this induced absorption is *not* observed in our experiment because CCS prevents the buildup of a sufficiently dense and narrow carrier distribution.

Additionally, Fig. 10 illustrates the strong influence of the CEF on the DTS; there is a strong induced transmission close above the band gap even without any band filling at the corresponding energies.

V. CONCLUSIONS

In conclusion, we present extensive experimental and theoretical data on carrier thermalization in intrinsic bulk GaAs at room temperature. Under these conditions, spectral-hole burning as well as coherent oscillations around the pump energy are observed for the first time. We find that the spectral-hole peak is initially centered at the excitation energy but shifts towards lower energies with increasing time delay. A negative transmission change above the spectral hole is found to be due to reflectivity changes. We find no significant dependence of electron-thermalization times on excitation energy and density. This observation is in good agreement with calculations of the plasma dynamics using dynamically screened particle interactions.

ACKNOWLEDGMENTS

The authors are grateful to A. Förster and H. Lüth (ISI-HL, KFA Jülich) for supplying the sample, and to K. Leo and H. J. Bakker for stimulating discussions. This work was supported by the Deutsche Forschungsgemeinschaft and the Alfried Krupp Stiftung.

[1] C. V. Shank, in *Ultrashort Laser Pulses and Applications*, edited by W. Kaiser (Springer, Berlin, 1988).
[2] J. Shah, Solid-State Electron. **32**, 1051 (1989).
[3] J. L. Oudar, D. Hulin, A. Migus, A. Antonetti, and F. Alexandre, Phys. Rev. Lett. **55**, 2074 (1985).
[4] W. H. Knox, C. Hirlimann, D. A. B. Miller, J. Shah, D. S. Chemla, and C. V. Shank, Phys. Rev. Lett **56**, 1191 (1986).
[5] W. H. Knox, D. S. Chemla, G. Livescu, J. E. Cunningham,

and J. E. Henry, Phys. Rev. Lett. **61**, 1290 (1988).
[6] W. Z. Lin, R. W. Schoenlein, J. G. Fujimoto, and E. P. Ippen, IEEE J. Quantum Electron. **QE-24**, 267 (1988).
[7] J. Nunnenkamp, J. H. Collet, J. Klebniczki, J. Kuhl, and K. Ploog, Phys. Rev. B **43**, 14 047 (1991).
[8] T. Gong, P. Mertz, W. L. Nighan, Jr., and P. M. Fauchet, Appl. Phys. Lett. **59**, 721 (1991).
[9] X. Q. Zhou, G. C. Cho, U. Lemmer, W. Kütt, K. Wolter, and H. Kurz, Solid-State Electron. **32**, 1591 (1989).
[10] T. Elsaesser, J. Shah, L. Rota, and P. Lugli, Phys. Rev. Lett. **66**, 1757 (1991).
[11] X. Q. Zhou, K. Leo, and H. Kurz, Phys. Rev. B **45**, 3886 (1992).
[12] R. Scholz, A. Stahl, X. Q. Zhou, K. Leo, and H. Kurz, IEEE J. Quantum Electron. **QE-28**, 2473 (1992).
[13] D. W. Snoke, W. W. Rühle, Y.-C. Lu, and E. Bauser, Phys. Rev. Lett. **68**, 990 (1992); Phys. Rev. B **45**, 10 979 (1992).
[14] P. C. Becker, H. L. Fragnito, C. H. Brito-Cruz, R. L. Fork, J. E. Cunningham, J. E. Henry, and C. V. Shank, Phys. Rev. Lett. **61**, 1647 (1988).
[15] J. Y. Bigot, M. T. Portella, J. W. Schoenlein, and C. V. Shank, Phys. Rev. Lett. **67**, 636 (1991).
[16] D. S. Kim, J. Shah, J. E. Cunningham, T. C. Damen, S. Schmitt-Rink, and W. Schäfer, Phys. Rev. Lett **68**, 2838 (1992).
[17] J. L. Oudar, A. Migus, D. Hulin, G. Grillon, J. Etchepare, and A. Antonetti, Phys. Rev. Lett. **53**, 384 (1984).
[18] M. T. Portella, J. Y. Bigot, R. W. Schoenlein, J. E. Cunningham, and C. V. Shank, Appl. Phys. Lett. **60**, 2123 (1992).
[19] P. C. Becker, H. L. Fragnito, C. H. Brito-Cruz, J. Shah, R. L. Fork, J. E. Cunningham, J. E. Henry, and C. V. Shank, Appl. Phys. Lett. **53**, 2089 (1988).
[20] R. G. Ulbrich, J. A. Kash, and J. C. Tsang, Phys. Rev. Lett. **62**, 949 (1989).
[21] J.-P. Foing, D. Hulin, M. Joffre, M. K. Jackson, J.-L. Oudar, C. Tanguy, and M. Combescot, Phys. Rev. Lett. **68**, 110 (1992).
[22] H. Haug, in *Optical Nonlinearities and Instabilities in Semiconductors*, edited by H. Haug (Academic, San Diego, 1988).
[23] H. Glaeske and M. Schubert, Phys. Status Soldi B **146**, 385 (1988).
[24] K. Henneberger and H. Haug, Phys. Rev. B **38**, 9759 (1988).
[25] S. Schmitt-Rink, D. S. Chemla, and H. Haug, Phys. Rev. B **37**, 941 (1988).
[26] R. Zimmermann, Phys. Status Solidi B **146**, 371 (1988).
[27] A. V. Kuznetsov, Phys. Rev. B **44**, 8721 (1991).
[28] F. Jahnke and K. Henneberger, Phys. Rev. B **45**, 4077 (1992).
[29] A. Stahl and I. Balslev, *Electrodynamics of the Semiconductor Band Edge* (Springer, Berlin, 1987).
[30] C. H. Brito-Cruz, J. P. Gordon, P. C. Becker, R. L. Fork, and C. V. Shank, IEEE J. Quantum Electron. **QE-24**, 261 (1988).
[31] J. Schlösser and A. Stahl, Phys. Status Solidi B **153**, 773 (1989).
[32] T. Kuhn and F. Rossi, Phys. Rev. Lett. **69**, 977 (1992); Phys. Rev. B **46**, 7496 (1992).
[33] J. H. Collet and T. Amand, Physica B **134**, 394 (1985); J. H. Collet, J. L. Oudar, and T. Amand, Phys. Rev. B **34**, 5443 (1986).
[34] J. H. Collet, Phys. Rev. B **47**, 10 279 (1993).
[35] R. Binder, D. Scott, A. E. Paul, M. Lindberg, K. Henneberger, and S. W. Koch, Phys. Rev. B **45**, 1107 (1992).
[36] P. Lugli, Appl. Phys. Lett. **50**, 1521 (1987).
[37] S. M. Goodnick and P. Lugli, Phys. Rev. B **37**, 2578 (1988).
[38] A. D. W. Bailey, C. J. Stanton, and K. Hess, Phys. Rev. B **42**, 3423 (1990).
[39] P. C. Becker, H. L. Fragnito, R. L. Fork, F. A. Beisser, and C. V. Shank, Appl. Phys. Lett. **54**, 411 (1988).
[40] T. F. Albrecht, K. Seibert, and H. Kurz, Opt. Commun. **84**, 223 (1991).
[41] J.-P. Foing, J.-P. Likforman, M. Joffre, and A. Migus, IEEE J. Quantum Electron. **QE-28**, 2285 (1992).
[42] R. Scholz, Ph.D. thesis, Rheinisch Westfälische Technische Hochschule Aachen, 1992.
[43] H. Heesel (unpublished).
[44] L. Banyai and S. W. Koch, Z. Phys. B **63**, 283 (1986).
[45] S. Schmitt-Rink, C. Ell, and H. Haug, Phys. Rev. B **33**, 1183 (1986).
[46] H. Haug and S. W. Koch, Phys. Rev. A **39**, 1887 (1989).
[47] R. Blank and H. Haug, Phys. Rev. B **44**, 10 513 (1991).
[48] R. Zimmermann, *Many-Particle Theory of Highly Excited Semiconductors* (Teubner, Leipzig, 1988).
[49] Y. H. Lee, A. Chavez-Pirson, S. W. Koch, H. M. Gibbs, S. H. Park, J. Morhange, A. Jeffery, L. Banyai, A. C. Gossard, and W. Wiegmann, Phys. Rev. Lett. **57**, 2446 (1986).
[50] M. Lindberg and S. W. Koch, Phys. Rev. B **38**, 7607 (1988).
[51] J. P. Sokoloff, M. Joffre, B. Fluegel, D. Hulin, M. Lindberg, S. W. Koch, A. Migus, A. Antonetti, and N. Peyghambarian, Phys. Rev. B **38**, 7615 (1988).
[52] D. C. Scott, R. Binder, and S. W. Koch, Phys. Rev. Lett. **69**, 347 (1992).
[53] J.-P. Foing, M. Joffre, M. K. Jackson, J.-L. Oudar, and D. Hulin, Phys. Status Solidi B **173**, 281 (1992).
[54] J. F. Young, P. J. Kelly, N. L. Henry, and M. W. C. Dharma-wardana, Solid State Commun. **78**, 343 (1991).
[55] N. S. Mansour, K. Diff, and K. F. Brennan, J. Appl. Phys. **70**, 6854 (1991).
[56] J.M. Wiesenfeld and A.J. Taylor, Phys. Rev. B **34**, 8740 (1986).
[57] H. Heesel, T. Zettler, A. Ewertz, and H. Kurz, in *Ultrafast Processes in Spectroscopy 1991*, edited by A. Laubereau and A. Selmeier, IOP Conf. Proc. No. 126 (Institute of Physics, Bristol, 1992); H. Heesel, S. Hunsche, A. Ewertz, H. Kurz, and T. Zettler, in *International Conference on Quantum Electronics Technical Digest Series 1992*, Vol. 9, p. 430.
[58] H.T. Grahn, C. Thomsen, and J. Tauc, Opt. Commun. **58**, 226 (1986).
[59] E. D. Palik, *Handbook of Optical Constants of Solids* (Academic Press, Orlando, 1985).
[60] R. Zimmermann, Phys. Status Solidi B **86**, K63 (1978).
[61] K. Arya and W. Hanke, Phys. Rev. B **23**, 2988 (1981).
[62] C. Tanguy and M. Combescot, Phys. Rev. Lett. **68**, 1935 (1992).